Materials Characterization 163 (2020): 110293

DOI: https://doi.org/10.1016/j.matchar.2020.110293

TiO_2 and Co multilayer thin films via DC Magnetron Sputtering at room temperature: Interface properties

Heiddy P. Quiroz[1], M. Manso-Silván[2], A. Dussan[1], Carlos Busó-Rogero[3], P. Prieto[4], F. Mesa[5*]

[1]*Universidad Nacional de Colombia - Bogotá, Dpto. de Física, Grupo de Materiales Nanoestructurados y sus Aplicaciones, Cra. 30 No. 45-03 Edificio 404 Yu Takeuchi Lab. 121C / 121B-1 Ciudad Universitaria – Bogotá, Postal Cod. 110001, Colombia.*

[2]*Departamento de Física Aplicada e Instituto de Ciencia de Materiales Nicolás Cabrera, Universidad Autónoma de Madrid, 28049 Madrid, Spain.*

[3]*Instituto Madrileño de Estudios Avanzados (IMDEA) Nanociencia, c./Faraday 9, Campus Universitario de Cantoblanco, E-28049 Madrid, Spain.*

[4]*Dpto. Física Aplicada M-12, Universidad Autónoma de Madrid, 28049, Madrid, Spain.*

[5] *Department of Biology, Faculty of Natural Sciences and Mathematics, Universidad del Rosario. Carrera 24 # 63C-69, Bogota D.C., 111221, Colombia*

** Corresponding author: e-mail: fredy.mesa@urosario.edu.co, Phone: +57 1 2970200 Ext. 4023.*

ABSTRACT

In this work, we prepared TiO_2 and Co multilayer thin films via DC magnetron sputtering method on (100) GaAs and (100) Si substrates. The power for each target (TiO_2 and Co), deposition time of the layers, and pressure during deposition were kept constant. From XRD, Raman, and IR measurements, the formation of the rutile and triclinic Co phases were identified in the multilayer thin films. An annealing process was carried *in situ* on all samples and subsequent to the deposition stage during 2 h. The substrate used was GaAs and Si wafer, favoring the formation and growth of the found phases. The diffusion and interdiffusion of the layers in the thin films were determined from Rutherford Backscattering Spectroscopy (RBS). In particular, Co and Ga were observed to associate after the annealing process according to the depth profiles. Due to the interdiffusion layers, the parallel magnetic contribution is not significant in the bilayer. Curves I-V of the Co/TiO_2 bilayer showed the presence of resistive switching, according to the bipolar resistive. A correlation between synthesis parameters and the physical properties of the multilayers is presented.

Key words: RBS, bilayer, multilayer, rutile, NVM, TiO_2

1. INTRODUCTION

The study of oxide heterostructures based on bilayers and multilayers has been of great interest in the last years due to the modification of magnetic, electrical, and optical properties [1-4]. However, the magnetic heterostructures are characterized by interface interaction between ferromagnetic and antiferromagnetic materials (metal or metallic alloys) [5,6] leaving a limited role to oxide semiconductors [4]. These properties have served as an impulse for the investigation of oxide semiconductors with magnetic properties [4]. This study of metal/semiconductor materials is of emerging relevance due to the physical properties of bilayer systems based on magnetic/non-magnetic materials. In fact, oscillatory interlayer exchange coupling (IEC) [7] or angular momentum current

effects have been evidenced into a non-magnetic layer by contribution of the ferromagnetic layer [8]. These phenomena have been observed in multilayer systems based in antiferromagnetic materials such as Cr or Mn [7, 9,10] and in ferromagnetic materials (Co, Cu and Fe) [11] with non-magnetic materials like Au, Mo, Pd and Ru [7,12]. More recently they have been also observed using semiconductors and insulators (ZnSe, Si, and MgO, respectively [7,13])

Semiconductors like CoO, Co_3O_4, TiO_2, ZnO, among others, exhibit magnetic properties: antiferromagnetic behavior in the case of cobalt oxide (CoO, Co_2O_3, Co_3O_4) [14], and diamagnetic behavior for TiO_2 or ZnO [15]. Nevertheless, the doping of oxide semiconductor matrices with transition metals allowed the contribution of magnetic behavior. In particular, Co-doped TiO_2 has been evidenced as a ferromagnetic material at room temperature [16, 17].

The properties of bilayer and multilayer structures depend on the synthesis method, thickness of the layers, and their crystallization. The study of the interface permitted the characterization and control over the thicknesses of individual layers, associated with the physical properties of these systems. Depending on these properties, the applications of these heterostructures have been directed to the Magnetic Random Access Memory (MRAM) [18], Resistivity Random Access Memory (RRAM) [19], spintronic materials [20], among others [21].

This work presents a structural, morphological, magnetic performance, and compositional study of TiO_2 and Co multilayer thin films, via DC magnetron Co-sputtering method at room temperature. Through Rutherford Backscattering Spectrometry, it was possible to establish the diffusion layers due to the annealing process and the in-depth profiles of the bilayer and multilayer thin films. The room temperature fabrication permitted to control the formation of the individual layers in the thin films, observed in the HR-SEM micrographs. Raman and XRD measurements proved the formation of rutile and Co phases in the thin films, without observing the formation of Cobalt oxides. I-V curves showed the potential application as Non-Volatile Memories (NVM) of the Co/TiO_2 bilayers.

2. MATERIALS AND METHODS

Co/TiO_2 multilayer thin films were deposited via DC magnetron sputtering on (100) GaAs and (100) Si wafer substrates using TiO_2 (99.9%) and Co (99.9%) targets. The targets were 762 mm diameter and 3 mm thickness. The substrate holder keeps static during deposition process and the sample size is 2.6 cm x 3.6cm. The target power (TiO_2 - 120 W and Co - 25 W), working pressure (2.5×10^{-2} Torr), deposition temperature T_s = 293 K and 473 K, and substrate-target distance (70 mm) parameters remained constant. The samples were annealed in situ at T_a = 473 K after the deposition process using IR lamps as heating source and PID control. Fig. 1 shows the schematic view of the bilayer and multilayer Co/TiO_2 thin films prepared, with a time sequence. In the case of bilayer structure, the deposition time was 30 min of TiO_2 and 5 min of Co, whilst, for the multilayer structure case was 10 min of TiO_2 and 5 min for each Co layer (cycling up to 6 layers).

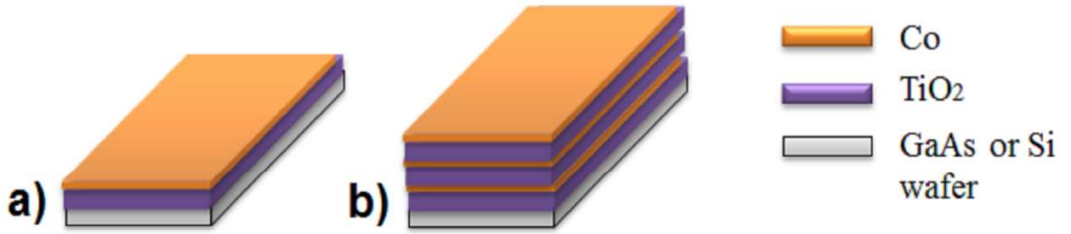

Figure 1. Schematic distribution of **a)** bilayer of Co/TiO_2 thin film, and **b)** 6 layers of TiO_2 and Co thin films.

The structural characterization of samples was realized through X-ray Diffraction (XRD), Raman and Rutherford Backscattering Spectrometry (RBS) measurements. Thin films were characterized through XRD measurements by using an EMPYREAN diffractometer by PANalytical with Pixcel 3D 2X2 detector of high speed, and 40 nm of depth in the 2θ range between 10° and 90°. The diffractometer was equipped with a Cu-Kα source: 1.540598 Å, voltage of 40 kV, and current of 40 mA. The software used for comparison was X'Pert High Score Plus by Rietveld refinement. Raman spectra were acquired at room temperature by using a Bruker Raman spectrometer SENTERRA model, with 532 nm laser excitation wavelength, focused on the sample by employing a 50x lens Olympus MPlan Achromat (0.75 NA). RBS measurements were performed using a Cockroft-Walton tandem linear accelerator with He^+ particles with an energy of 2 MeV and 3.035 MeV (this latter condition, to resonantly enhance the scattering cross-section of oxygen atoms). Si planar detectors collect the backscattered particles from the sample at an angle of 170° with a normal incident and a mobile detector of 195°. RBS analysis was done by using the SIMNRA simulation software package.

The morphological characterization of the samples was carried out in a scanning electron microscope Phillips XL 30S FEG with an acceleration voltage of 10 kV in a high vacuum regime (~10^{-6} mbar). Additionally, the angular dependence of the magnetization was measured at room temperature by vectorial-Kerr magneto-optical in a longitudinal configuration, with a maximum magnetic field of 110 mT.

3. RESULTS AND ANALYSIS

Fig. 2 shows the XRD patterns of Co/TiO_2 bilayers and multilayer with GaAs and Si substrate. In the case of the bilayer, it is possible to observe the formation of the rutile phase (PDF 01-088-1172) and Co crystals (PDF 96-410-5681). Meanwhile, Co/TiO_2 multilayers on GaAs present the anatase phase with principal peak located in 25.68°, associated to (011) plane. The presence of these phases and growth plane ([011]) are in agreement with the structure and orientation of GaAs and Si wafer. The Co has a triclinic structure associated with the contribution of TiO_2 in the growth of the bilayer. Nevertheless, this structure is not stable [22], and diffusion of the Co layer into TiO_2 was observed in the multilayer thin films.

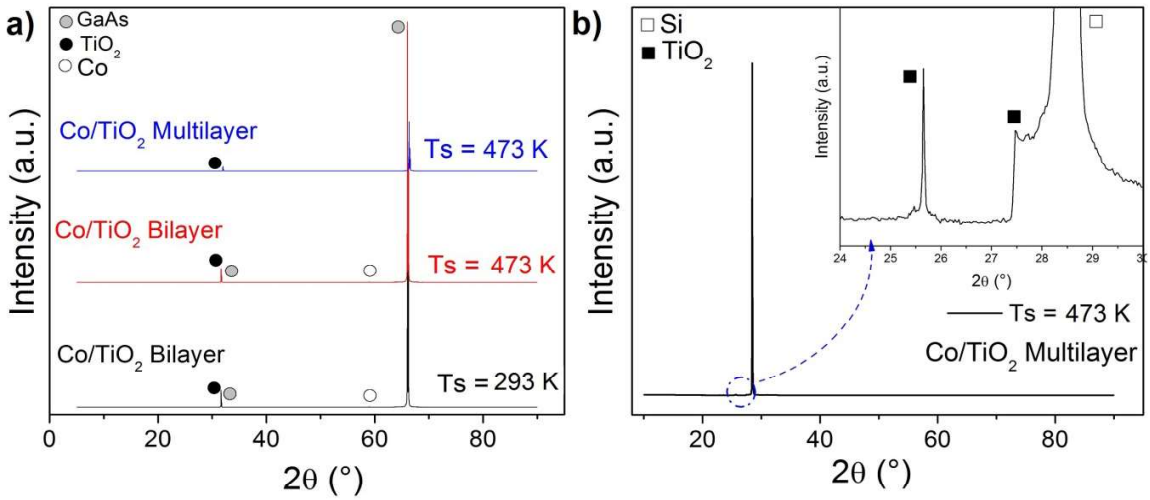

Figure 2. XRD patterns of **a)** Co/TiO_2 bilayers and multilayers on GaAs substrate varying T_s and **b)** Co/TiO_2 multilayer on Si substrate at T_s = 473K.

The interdiffusion layer, in the multilayer samples deposited on GaAs and Si substrates, (Fig. 2a and b) was possible to associate when is identified for the TiO_2 phase and not for Co oxide or Co crystals phases. The diffusion is due to deposition temperature (T_s = 473 K) and annealing process after deposition (473 K for 2 h).

Raman measurements evidenced the formation of rutile phases in the Co/TiO_2 bilayer on Si, in agreement with the XRD patterns. Fig. 3 shows the Raman peaks associated with the rutile phases with A_{1g} and E_g modes, located at 618 cm^{-1} and 449 cm^{-1}, respectively [23].

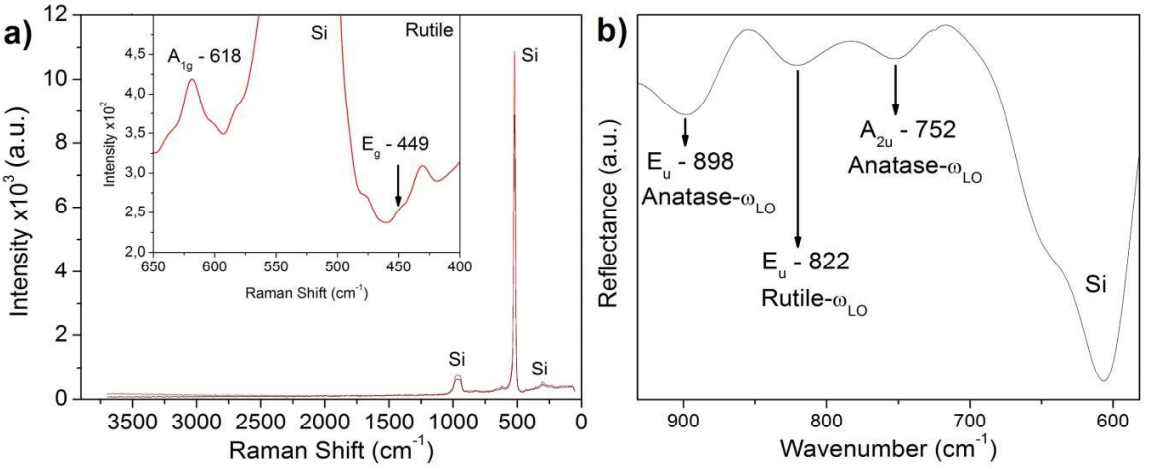

Figure 3. a) Raman spectrum of Co/TiO_2 bilayer with T_s = 473 K, and **b)** IR spectrum of Co/TiO_2 multilayer with T_s = 473 K.

However, in the Co/TiO_2 multilayers with T_s = 473 K we identified the E_u and A_{2u} (ω_{LO}) longitudinal optical modes characteristic of the anatase phase in the IR spectrum (Fig 3b), which are located at 898 cm^{-1} and 752 cm^{-1}, respectively. Additionally, the mode located at

822 cm^{-1} confirms the presence of the rutile phase (Eq. 1). For the rutile phase the space group is $P4_2/mnm$ and the optical modes in Γ point are [24]:

$$\Gamma_{\acute{o}pt} = A_{1g} + A_{2g} + A_{2u} + B_{1g} + 2B_{2u} + B_{2g} + E_g + 3E_u \quad (1)$$

where g represents the Raman active modes, u the IR active modes, and E the degenerate modes. In Fig 3b it is possible to observe the IR spectrum of Co/TiO_2 multilayer, evidencing the formation of TiO_2 polymorphs. The presence of these TiO_2 polymorphs is associated to the synthesis method and deposition temperature, according to the anatase-rutile phase transition [25]. The transition is reported around 573 K in atmospheric pressure [25]. However, the substrate temperature was 473 K, which is not enough to achieve a complete anatase-rutile transformation. Additionally, the Raman and IR spectra show shifts and widening peaks due to the lattice defects by Co diffusion into TiO_2 layer [26,27] (see Table 1).

Fig. 4 presents 2 MeV He^{2+} RBS spectra of the Co/TiO_2 bilayer deposited on GaAs with T_s = 293 K and 473 K (a and b, respectively). The simulated RBS spectra allowed estimating the layer formation, species diffusion, and layer depth profile. This technique has been reported in the M. S. Hussain, et al. study of the multilayers thin films of TiO_2 and Ge [28], and multilayers thin films of Co/Cu with magnetic properties for R. Nagel, et al. [29], both synthesized by electron-beam evaporation. However, the study of diffusion and layer formation of Co/TiO_2 multilayer by DC magnetron co-sputtering for spintronic application, it is still under investigation.

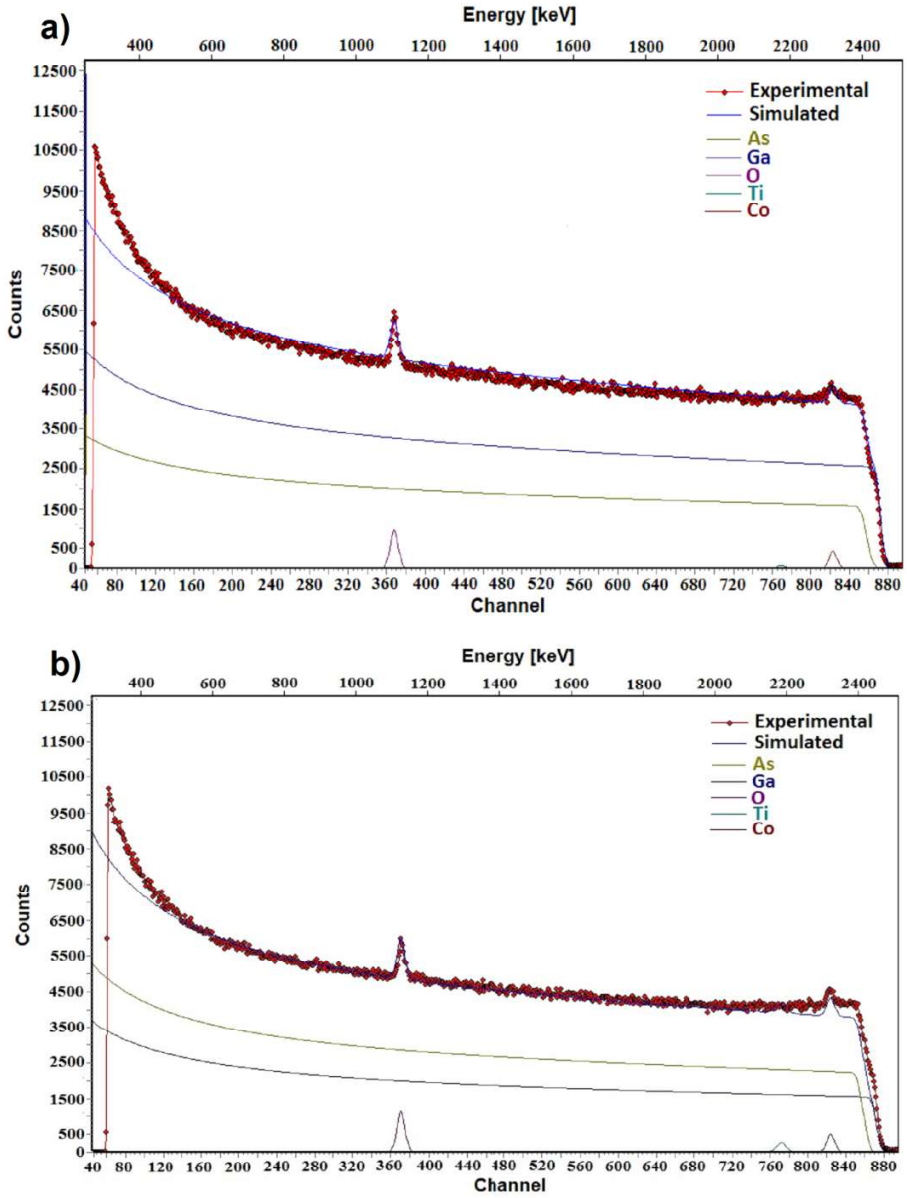

Figure 4. Experimental (dotted lines) and simulated (straight lines) RBS spectra of Co/TiO_2 bilayer deposited on GaAs with **a)** T_s = 293 K, and **b)** T_s = 473 K.

The fitting of the spectra is performed by multiple dispersions of different elements and thickness of the sample (Fig. 4). Peaks of the Ti, Co, and O elements for the Co/TiO_2 bilayer, and GaAs corresponding to the substrate, were identified.

In the region between 2400 keV and 2500 keV, it is possible to observe a decrease of the counts and a small step, associated with the thin films-substrate transition. The changes in the spectra and decrease of the counts permitted to determine the constitution of the layer. Table 1 shows the depth profile and relationship with the thickness of the layer, through SEM measurements.

Table 1. The depth profile of Co/TiO_2 bilayers varying the substrate temperature.

	Layer	Thickness - RBS ($10^{15}\ atoms/cm^2$)	Thickness - SEM (nm)
T_s = 293K	Co-O	25	-
	Co	80	75.50
	TiO_2	145	68.95
T_s = 473K	TiO_2-Co	150	127.30
	Ga-O	160	-

The formation of thin Co oxide with $25 \times 10^{15} atoms/cm^2$ of thickness was identified in the case of the Co/TiO_2 bilayer with T_s = 293 K. This small layer was not observed in the HR-SEM or XRD measurements because of the first Co oxidation layer on the surface. In comparison, in the bilayer with T_s = 473 K, the diffusion of the layer was observed (Fig. 5) with a thickness of $1.5 \times 10^{17} atoms/cm^2$. Additionally, the presence of a Ga-O layer of $2.6 \times 10^{16} atoms/cm^2$ thickness associated with the deposition temperature and annealing process was determined in the RBS spectrum.

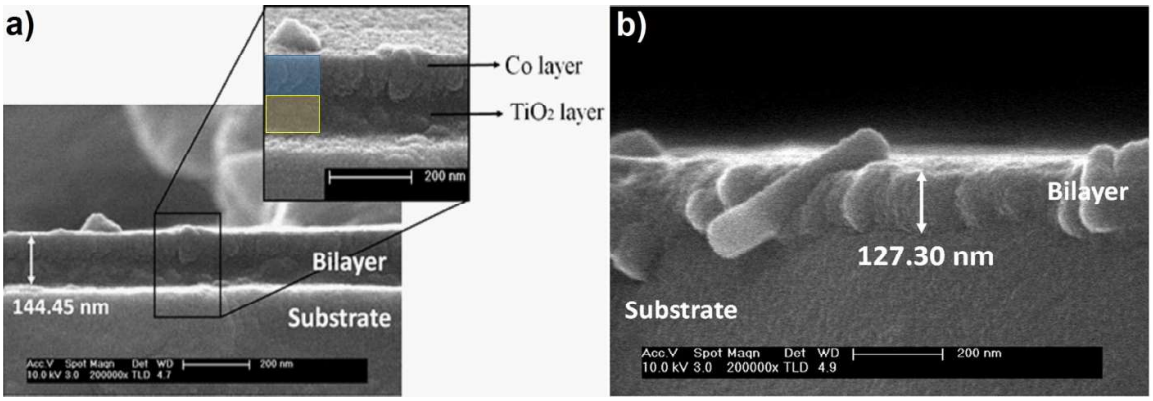

Figure 5. HR-SEM micrograph of Co/TiO_2 Bilayer thin films with **a)** T_s = 293 K. Inset shows the layer of the thin film with annealing process, and **b)** T_s = 423 K.

Fig. 5 shows the HR-SEM micrographs for the Co/TiO_2 bilayer thin films with a variation of the deposition temperature. In the bilayer with T_s = 293 K, the alternation is very clear with 144.45 ± 7.86 nm thickness of the whole thin film, where the Co layer has a thickness of 75.50 ± 1.52 nm. It is possible to observe the diffusion of the Co layer into the TiO_2 layer (inset Fig. 5a), associated with the annealing process. In comparison with the bilayer of T_s = 423 K (Fig. 5b), the diffusion of both layers and formation of compact "blocks" is observed, according to the MD model [21].

The diffusion of the initial layer is observed (Fig. 6) in the case of the multilayers with T_s = 293 K and annealing process (T_a = 473 K). However, the last layers of the Co and TiO_2 were identified with a thickness of 87.08 ± 1.73 nm and 98.36 ± 4.93 nm, respectively. Additionally, in the multilayered and bilayer thin films (Fig. 5 and 6) was observed the presence of grains in the surface, associated with the nucleation process of Co.

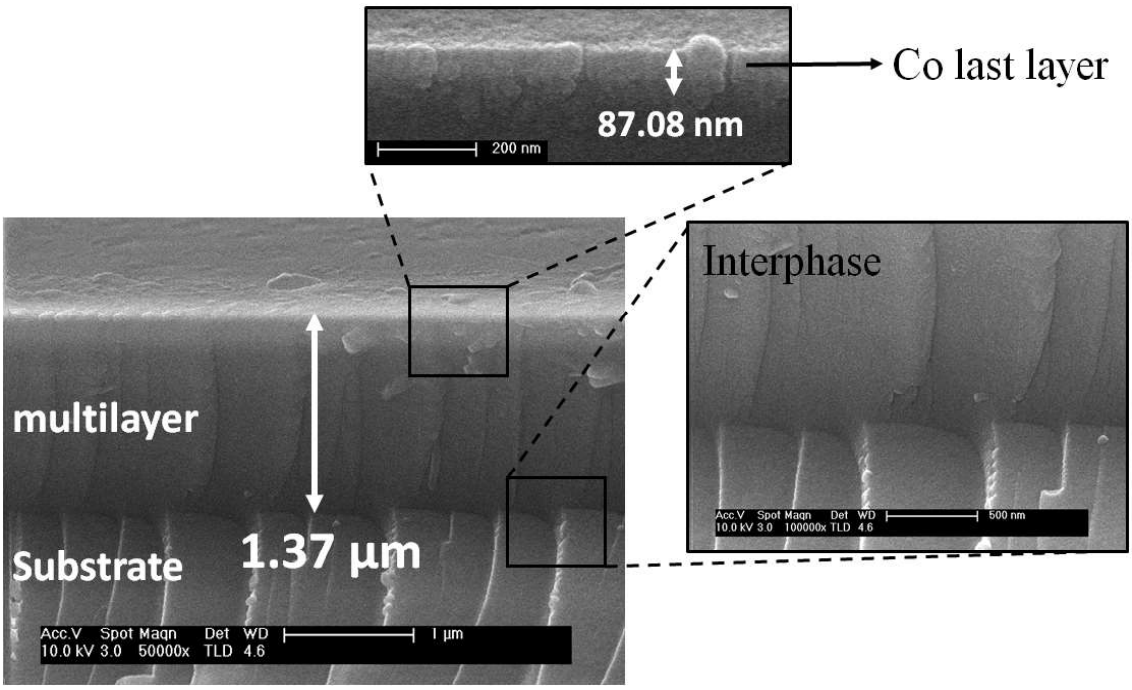

Figure 6. HR-SEM micrograph of Co/TiO_2 multilayer thin film with annealing process at 473K. Inset shows Co last layer and interphase of the thin film and substrate.

The identification of interdiffusion and diffusion layers has been observed, according to the formation of thin films and synthesis method (Inset Fig. 5 and Fig. 6). The interdiffusion effect is an important characteristic of the multilayer systems since this affects the magnetic behavior due to the magnetic anisotropy at the interfaces [22]. The magnetic multilayer structures can be modified the magnetic behavior if in which magnetic layers are separated by non-magnetic layers [30-34]. The control of thickness in non-magnetic layers is very important just as the magnetic interaction, magnetic anisotropy, interface interaction, among others [36-37]. Fig. 7 shows the in-plane hysteresis loops for α_H = 0 and 27º for the Co/TiO_2 bilayer sample, with T_s = 293 K measure at RT. The angle α_H represents the in-plane angular rotation of the sample, respect to a fixed external magnetic field direction. The sample presents an in-plane magnetic isotropic behavior, mainly observed in polycrystalline films.

If the interdiffusion between layers is small and the layers are well defined (as the sample with the RBS depth profile in Table 1), the magnetic isotropic is not significant [22]. Therefore, the changes in the angle of the applied field do not affect the hysteresis loop shape or behavior of the normalized intensity as a function of the applied field (Inset Fig. 7). This behavior can be modified in the case of multilayers [22] due to the diffusion of the layers (Fig. 6).

Additionally, the thickness of the magnetic layer is proportional to the diameter of the diffusion zone (TiO_2 semiconductor layer), which can also account for linear behavior when the angle is modified. This behavior was favored to the structural formation of the phases in the Co/TiO_2 bilayer. Hence, the rutile structure and deposition temperature

contributed to the formation of triclinic Co on the surface (Fig. 1). The triclinic Co has not an easy axis of magnetization in comparison with a hexagonal structure, which has two axes (easy and hard). Therefore, the Co layer did not contribute to the magnetic isotropic behavior.

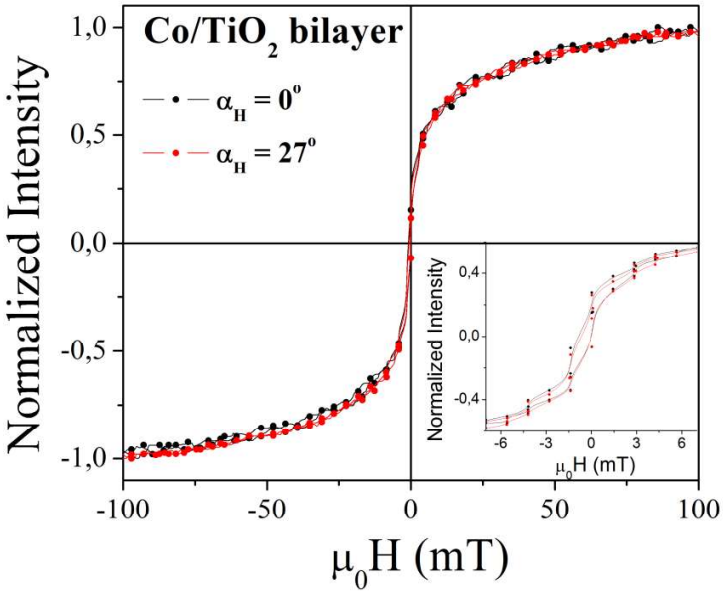

Figure 7. Magnetization loops at room temperature acquired at α_H = 0° and α_H = 27° of Co/TiO_2 bilayer sample, with T_s = 293 K.

Figure 8 shows the curves I-V of the Co/TiO_2 bilayer at T_s = 293 K on titanium sheet substrate as bottom contact, and the Co layer like top contact. The range of applied voltage was varied between -0.3 V to 0.3 V and -3 V to 3 V to evidence the behavior of the hysteresis loop or curve butterfly type [19]. The architecture of non-volatile memory based on resistive change is characteristic of metal/insulator or oxide/metal [20-22]; in this case, $Co/TiO_2/Ti$ configuration is proposed.

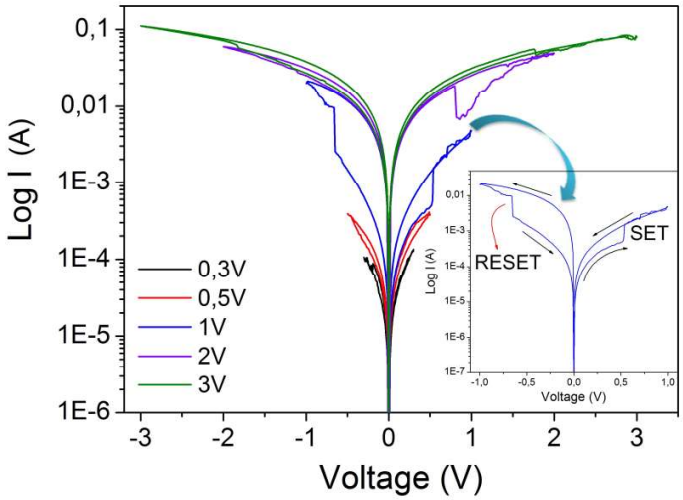

Figure 8. I-V curves of the Co/TiO_2 bilayer with T_s = 293 K.

Therefore, it is possible to observe that the switching effect occurs from HRS - high resistive state to LRS - low resistive state (known as SET) in the positive voltage region, and the LRS to HRS (RESET) or reversible resistance switching, in the negative voltage region (Inset Fig. 8). This behavior is associated to bipolar resistive switching, where the formation of the conductive filaments occurs in the RESET state [19]. Hence, the Co/TiO_2 bilayer is a promising material for RRAM - resistive random access memories in comparison with reported architectures, using the Co layer like top contact and TiO_2 layer as insulator matrix, in the fabrication of RRAM systems.

Conventional configuration for RRAM is based on Metal/Semiconductor or Insulator/Metal architecture; however, there are studies of metal oxides like semiconductors with a higher bandgap, such as NiO [38], TiOx [39], CuO_x [40], among others [41]. In these cases, Au, Ag, or C top contact was used while the upper contact was ITO, Au, or FTO [38-43]. This results (I-V measurements) evidence the potential application of bilayer and multilayer systems in the fabrication of the RRAM's using the Co top layer like contact and a Ti sheet like upper contact.

4. CONCLUSION

In this work, TiO_2/Co bilayers and multilayers were fabricated via DC magnetron co-sputtering method, varying substrate temperature. The formation of the rutile phase and Co of the triclinic structure were observed from XRD, Raman, and IR. A study of the RBS spectra showed the diffusion of the layers when the deposition temperature was increased; additionally, the formation of the small Co oxide and Ga-O layers, in the bilayer and multilayer, were observed. The layers' diffusion in thin films was identified through the HRSEM. When the deposition temperature was 293 K for the TiO_2/Co bilayer, the observed interdiffusion was between Co and TiO_2 layers. According to the triclinic structure of Co this can be favored by the presence of the rutile layer, it was possible to ascertain that magnetic isotropic behavior is not significant in the Co/TiO_2 bilayer sample with T_s = 293 K. The architecture of the Co/TiO_2 bilayer shows promising properties for its application in RRAM associated with the behavior of resistive switching bipolar.

ACKNOWLEDGMENTS

Heiddy Paola Quiroz is scholarship researcher of Doctorados Colciencias Conv. 727 - 2015. Special acknowledgments to the professor Pilar Prieto Recio of Universidad Autónoma de Madrid.

REFERENCES

[1] M. I. Khan, Synthesis, characterization and application of Co doped TiO_2 multilayer thin films, Results Phys. 9 (2018) 359–363. https://doi.org/10.1016/j.rinp.2018.02.068.
[2] Marikkannan Murugesan, Dinesh Arjunraj, J. Mayandi, Vishnukanthan Venkatachalapathy, J. M. Pearce, Properties of Al-doped zinc oxide and In-doped zinc

oxide bilayer transparent conducting oxides for solar cell applications, Mater. Lett. 222 (2018) 50-53. https://doi.org/10.1016/j.matlet.2018.03.097.
[3] R. K. Gupta, K.Ghosh, P. K. Kaho, Room temperature ferromagnetic multilayer thin film based on indium oxide and iron oxide for transparent spintronic applications, Mater. Lett. 64 (2010) 2022-2024. https://doi.org/10.1016/j.matlet.2010.06.026.
[4] Frances Hellman, Rev. Mod. Phys. 89 (2017) 025006-1 - 025006-79.
[5] P. Borisov, W. Kleemann, Exchange bias and ferromagnetic coercivity in heterostructures with antiferromagnetic Cr_2O_3, J. Appl. Phys. 110 (2011) 033917. https://doi.org/10.1063/1.3621460.
[6] Grace L Causer, Hanliang Zhu, Mihail Ionescu, Gary J Mankey, Xiaolin L. Wang, Frank Klose, Tailoring exchange bias in ferro/antiferromagnetic $FePt_3$ bilayers created by He^+ beams, J. Phys.: Condens. Matter 30 (2018) 315804. https://doi.org/10.1088/1361-648X/aad075.
[7] Z. Kurant, M. Tekielak, I. Sveklo, A. Wawro, A. Maziewski, Interlayer coupling-driven magnetic ordering and magnetization processes in ultrathin Au/Co/Mo/Co/Au film, J. Magn. Magn. Mater. 475 (2019) 683–694. https://doi.org/10.1016/j.jmmm.2018.12.015.
[8] H. Vigo-Cotrina, A. P. Guimarães, Parallels between a system of coupled magnetic vortices and a ferromagnetic/nonmagnetic (FM/NM) multilayer system, J. Magn. Magn. Mater. 497 (2020) 166009. https://doi.org/10.1016/j.jmmm.2019.166009.
[9] A.C. Daykin, J.P. Jakubovics, A.K. Petford-Long, A study of interlayer exchange coupling in a Co/Cr/Co trilayer using transmission electron microscopy, J. Appl. Phys. 82 (1997) 2447–2452. https://doi.org/10.1063/1.366054.
[10] B. Zhang, C. Bin Wu, W. Kuch, Tailoring interlayer coupling and coercivity in Co/Mn/Co trilayers by controlling the interface roughness, J. Appl. Phys. 115 (2014). https://doi.org/10.1063/1.4884235.
[11] A. Subbotin, E. M. Pashaev, A. L. Vasiliev, Yu. M. Chesnokov, G. V. Prutskov, E. A. Kravtsov, M. V. Makarova, V. V. Proglyado, V. V. Ustinov, The influence of microstructure on perpendicular magnetic anisotropy in Co/Dy periodic multilayer systems, Physica B Condens. Matter 573 (2019) 28-35. https://doi.org/10.1016/j.physb.2019.06.044.
[12] Z.Q. Qiu, J. Pearson, S.D. Bader, Oscillatory interlayer magnetic coupling of wedged Co/Cu/Co sandwiches grown on Cu(100) by molecular beam epitaxy, Phys. Rev. B. 46 (1992) 8659–8662, https://doi.org/10.1103/PhysRevB.46.8659.
[13] M. Luoa, Y.H. Shen, Carrier-mediated antiferromagnetic interlayer exchange coupling in Ga co-doped (Zn, Ni)O-based multilayers, Optik 127 (2016) 10705–10709. http://dx.doi.org/10.1016/j.ijleo.2016.08.108.
[14] Xuemin He, Huigang Shi, Synthesis and anomalous magnetic properties of hexagonal CoO nanoparticles, Mater. Res. Bull. 46 (2011) 1692-1697. http://dx.doi.org/10.1016/j.materresbull.2011.05.037.
[15] B. Anitha, M. AbdulKhadar, AlokBanerjee, Paramagnetic behavior of Co doped TiO_2 nanocrystals controlled by self-purification mechanism, J. Solid State Chem. 239 (2016) 237–245. https://doi.org/10.1016/j.jssc.2016.04.035.
[16] Y. B. Lin, Y. M. Yang, B. Zhuang, S. L. Huang, L. P. Wu, Z. G. Huang, F. M. Zhang, Y. W. Du, Ferromagnetism of Co-doped TiO2 films prepared by plasma enhanced chemical vapour deposition (PECVD) method, J. Phys. D: Appl. Phys. 41 (2008) 195007. doi:10.1088/0022-3727/41/19/195007.

[17] Qing Wang, Xiaoming Liu, XuegangWei, Jianfeng Dai, Weixue Li, Ferromagnetic Property of Co and Ni Doped TiO_2 Nanoparticles, J. Nanomaterials 371582 (2015) 1-6. http://dx.doi.org/10.1155/2015/371582.
[18] An Chen, A review of emerging non-volatile memory (NVM) technologies and applications, Solid-State Electron. 125 (2016) 25–38. https://doi.org/10.1016/j.sse.2016.07.006.
[19] Shi-Xiang Chen, Sheng-Po Chang, Shoou-Jinn Chang, Wei-Kang Hsieh, and Cheng-Han Lin, Highly Stable Ultrathin TiO_2 Based Resistive Random Access Memory with Low Operation Voltage, ECS J. Solid State Sci. Technol., 7 (2018) Q3183-Q3188. doi: 10.1149/2.0281807jss.
[20] Shimeng Yu, Resistive Random Access Memory (RRAM) From Devices to Array Architectures, Morgan & Claypool Publishers, Arizona, 2016.
[21] Pierre Camille Lacaze, Jean-Christophe Lacroix, Non-volatile Memories, Wiley, Hoboken, 2014.
[22] Ke-Jing Lee, Yu-Chi Chang, Cheng-Jung Lee, Li-Wen Wang, Yeong-Her Wang, 1T1R Nonvolatile Memory with Al/TiO_2/Au and Sol-Gel-Processed Insulator for Barium Zirconate Nickelate Gate in Pentacene Thin Film Transistor, Mater. 10 (2017) 1408. doi: 10.3390/ma10121408.
[23] I. Lukačević, S. K. Gupta, Prafulla K. Jha, D. Kirin, Mater. Chem. Phys. 137 (2012) 282-289. https://doi.org/10.1016/j.matchemphys.2012.09.022.
[24] M. Giarola, A. Sanson, F. Monti, G. Mariotto, Phys. Rev. B 81 (2010) 174305. https://doi.org/10.1103/PhysRevB.81.174305
[25] C.N.R. Rao, G. V. Subba Rao, Transition Metal Oxides - Crystal chemistry, phase transition and related aspects, U.S. Department of Commerce, National Bureau of Standards, Michigan, 1974.
[26] Hong Zhang, Xinhua Ouyang, Bo Yang, Ryan Lutes, Yonghao Ni, Ceram. Int. 44 (2018) 6362–6369. https://doi.org/10.1016/j.ceramint.2018.01.027.
[27] Hongye Zhang, Tianhao Ji, Yifan Liu, Jianwang Cai, J. Phys. Chem. 112 (2008) 8604–8608. https://doi.org/10.1021/jp8003294.
[28] Mirza Sajjad Hussain, Mazhar Mehmood, Jamil Ahmad, M. Tauseef Tanvia, A. Faheem Khan, Turab Ali, Arshad Mahmood, Mater. Chem. Phys. 139 (2013) 17-26. http://dx.doi.org/10.1016/j.matchemphys.2012.10.037.
[29] R. Nagel, C. Alof, A. G. Balogh, W. M. Arnoldbik, D. O. Boerma, Nucl. Instrum. Methods Phys. Res., Sect. B. 183 (2001) 140-145. https://doi.org/10.1016/S0168-583X(01)00320-2.
[30] Pavel V. Prudnikov, Vladimir V. Prudnikov, Marina V. Mamonova, Natalia I. Piskunova, J. Magn. Magn. Mater. 482, (2019) 201-205. https://doi.org/10.1016/j.jmmm.2019.03.061.
[31] P. Grünberg, R. Schreiber, Y. Pang, M.B. Brodsky, H. Sowers, Phys. Rev. Lett. 57 (1986), 2442-2445. https://doi.org/10.1103/PhysRevLett.57.2442.
[32] M.N. Baibich, J.M. Broto, A. Fert, et al. Phys. Rev. Lett. 61 (1988) 2472-2475. https://doi.org/10.1103/PhysRevLett.61.2472.
[33] A. Barthelemy, A. Fert, Phys. Rev. B. 43 (1991) 13124-13129. https://doi.org/10.1103/PhysRevB.43.13124.
[34] S.S.P. Parkin, Annu. Rev. Mater. Sci., 25 (1995) 357-388. https://doi.org/10.1146/annurev.ms.25.080195.002041.

[35] P.V. Prudnikov, V.V. Prundikov, M.A. Medvedeva, JETP Lett. 100 (2014) 446-450. Doi: 10.1134/S0021364014190096.
[36] A. Pelissetto, E. Vicari, Phys. Rep. 368 (2002) 549-727. https://doi.org/10.1016/S0370-1573(02)00219-3.
[37] B. Heinrich, T. Monchesky, R. Urban, J. Magn. Magn. Mater. 236 (2001) 339-346. https://doi.org/10.1016/S0304-8853(01)00455-3.
[38] S. Seo, M. J. Lee, D. H. Seo, E. J. Jeoung, D.-S. Suh, Y. S. Joung, I. K. Yoo, I. R. Hwang, S. H. Kim, I. S. Byun, J.-S. Kim, J. S. Choi, B. H. Park, Appl. Phys. Lett. 85 (2004) 5655-5657. https://doi.org/10.1063/1.1831560.
[39] B. J. Choi, D. S. Jeong, S. K. Kim, C. Rohde, S. Choi, J. H. Oh, H. J. Kim, C. S. Hwang, K. Szot, R. Waser, B. Reichenberg, S. Tiedke, J. Appl. Phys. 98 (2005) 033715. https://doi.org/10.1063/1.2001146.
[40] A. Chen, S. Haddad, Y. J. Wu, T. Fang, Z. Lan, S. Avanzino, M. Buynoski, M. Rathor, W. D. Cai, N. Tripsas, C. Bill, M. Vanbuskirk, M. Taguchi, IEEE International Electron Devices Meeting. (2005) 746-749. Doi: 10.1109/IEDM.2005.1609461.
[41] Shimeng Yu, Resistive random access memory (RRAM) from devices to array architectures, Morgan & Claupool Publisher, USA, 2016.
[42] I. Valov, R. Waser, J. R. Jameson, M. N. Kozicki, Nanotechnology, 22 (2011) 254003, Doi: 10.1088/0957-4484/22/25/254003.
[43] Shi-Xiang Chen, Sheng-Po Chang, Shoou-Jinn Chang, Wei-Kang Hsieh, Cheng-Han Lin, ECS J. Solid State Sci. Technol. 7 (2018) Q3183-Q3188. Doi: 10.1149/2.0281807jss.

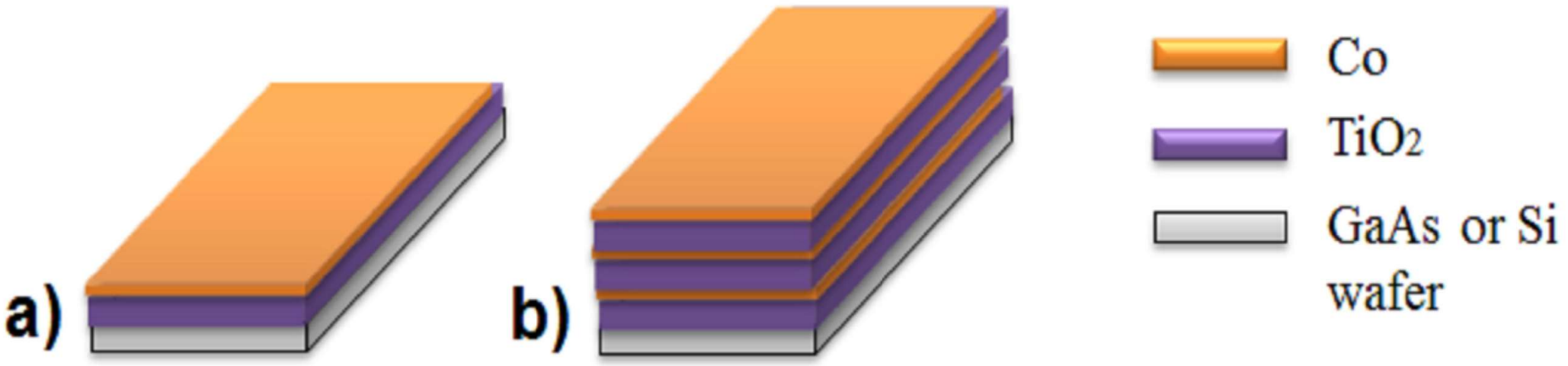
a)
b)
Co
TiO2
GaAs or Si wafer

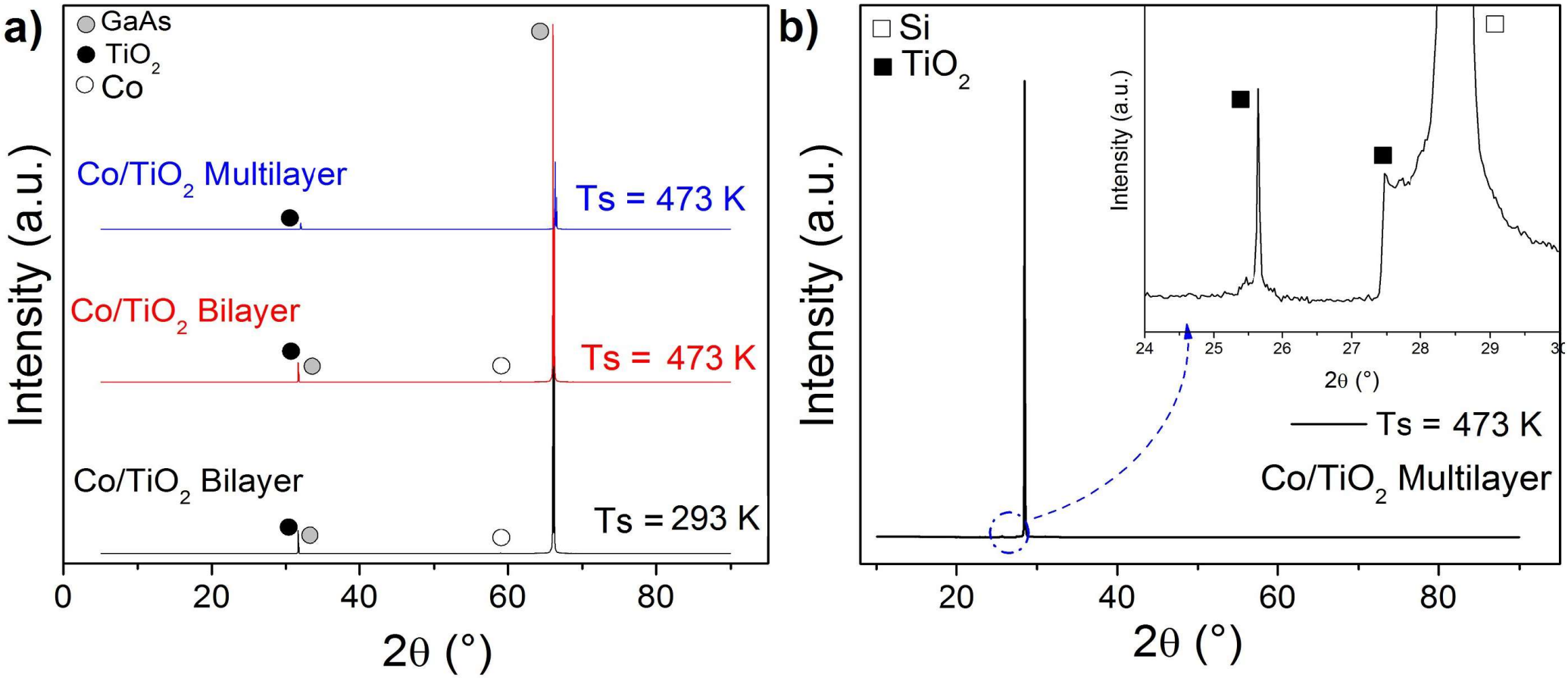
a)
GaAs
TiO2
Co
Co/TiO2 Multilayer
Ts = 473 K
Co/TiO2 Bilayer
Ts = 473 K
Co/TiO2 Bilayer
Ts = 293 K
Intensity (a.u.)
0
20
40
60
80
2θ (°)
b)
Si
TiO2
Intensity (a.u.)
24
25
26
27
28
29
2θ (°)
Ts = 473 K
Co/TiO2 Multilayer
Intensity (a.u.)
20
40
60
80
2θ (°)

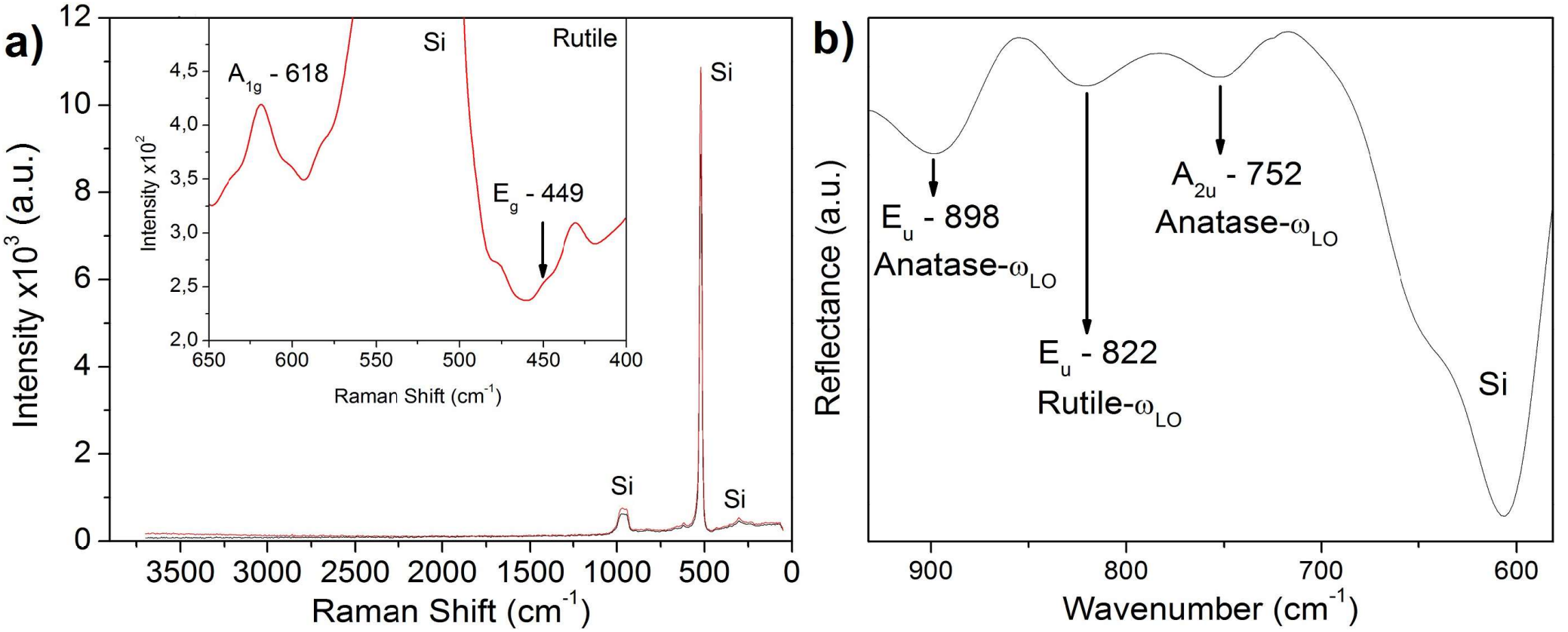
a)
Intensity x10^3 (a.u.)
Raman Shift (cm^-1)
Si
Si
Si
Rutile
A1g - 618
Eg - 449
Intensity x10^2
Raman Shift (cm^-1)
b)
Reflectance (a.u.)
Eu - 898
Anatase-ωLO
Eu - 822
Rutile-ωLO
A2u - 752
Anatase-ωLO
Si
Wavenumber (cm^-1)

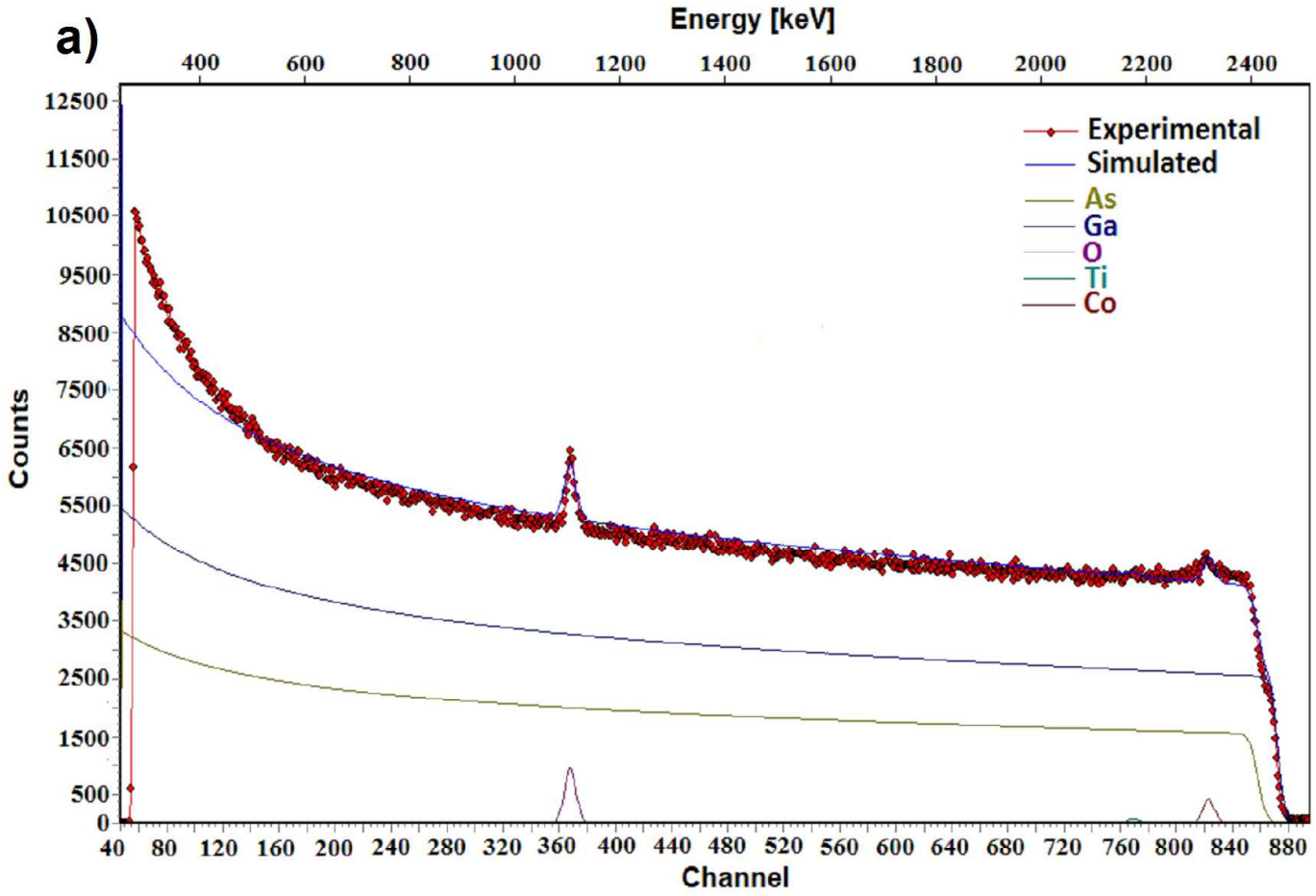
a)
Energy [keV]
400 600 800 1000 1200 1400 1600 1800 2000 2200 2400
Experimental
Simulated
As
Ga
O
Ti
Co
Counts
12500 11500 10500 9500 8500 7500 6500 5500 4500 3500 2500 1500 500 0
40 80 120 160 200 240 280 320 360 400 440 480 520 560 600 640 680 720 760 800 840 880
Channel

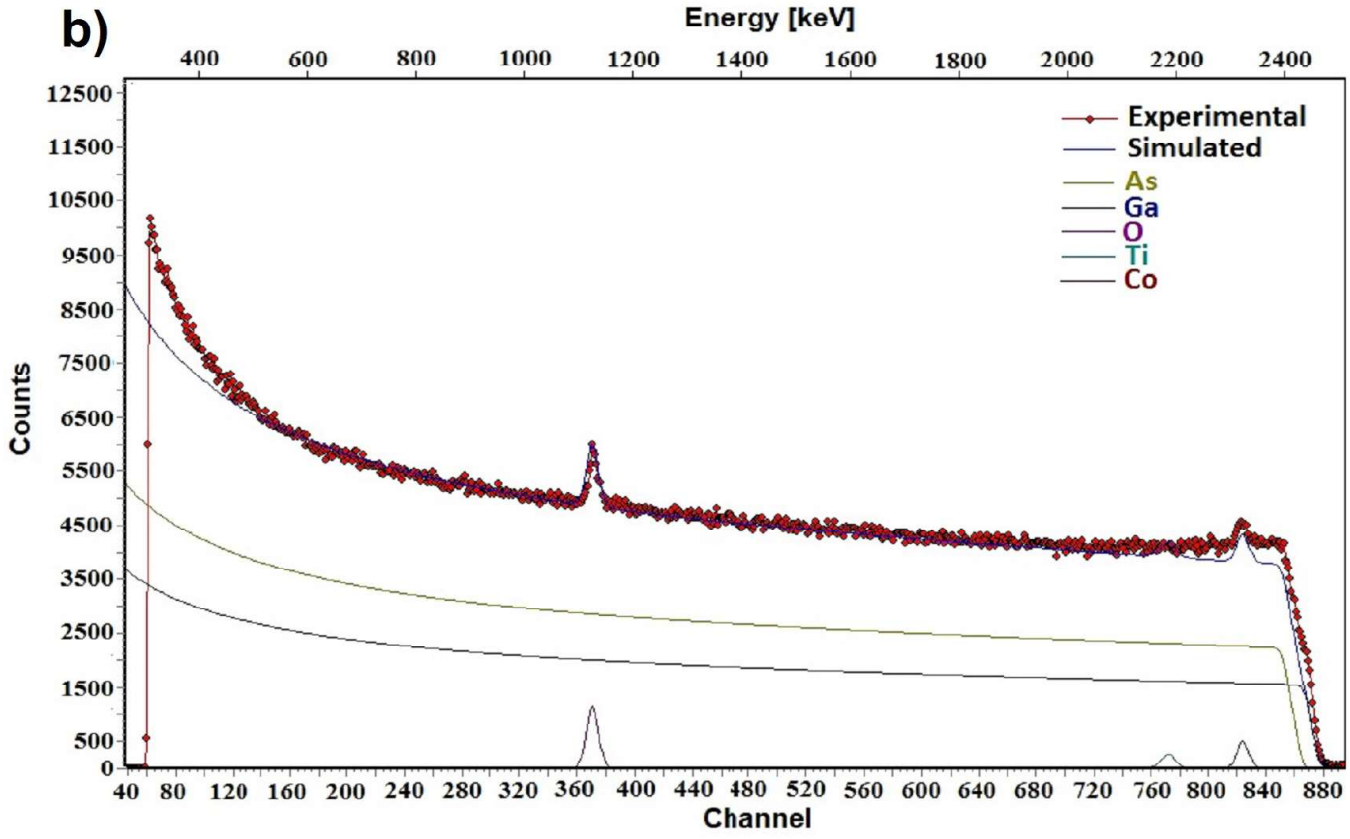
b)
Energy [keV]
400 600 800 1000 1200 1400 1600 1800 2000 2200 2400
Experimental
Simulated
As
Ga
O
Ti
Co
Counts
12500 11500 10500 9500 8500 7500 6500 5500 4500 3500 2500 1500 500 0
40 80 120 160 200 240 280 320 360 400 440 480 520 560 600 640 680 720 760 800 840 880
Channel

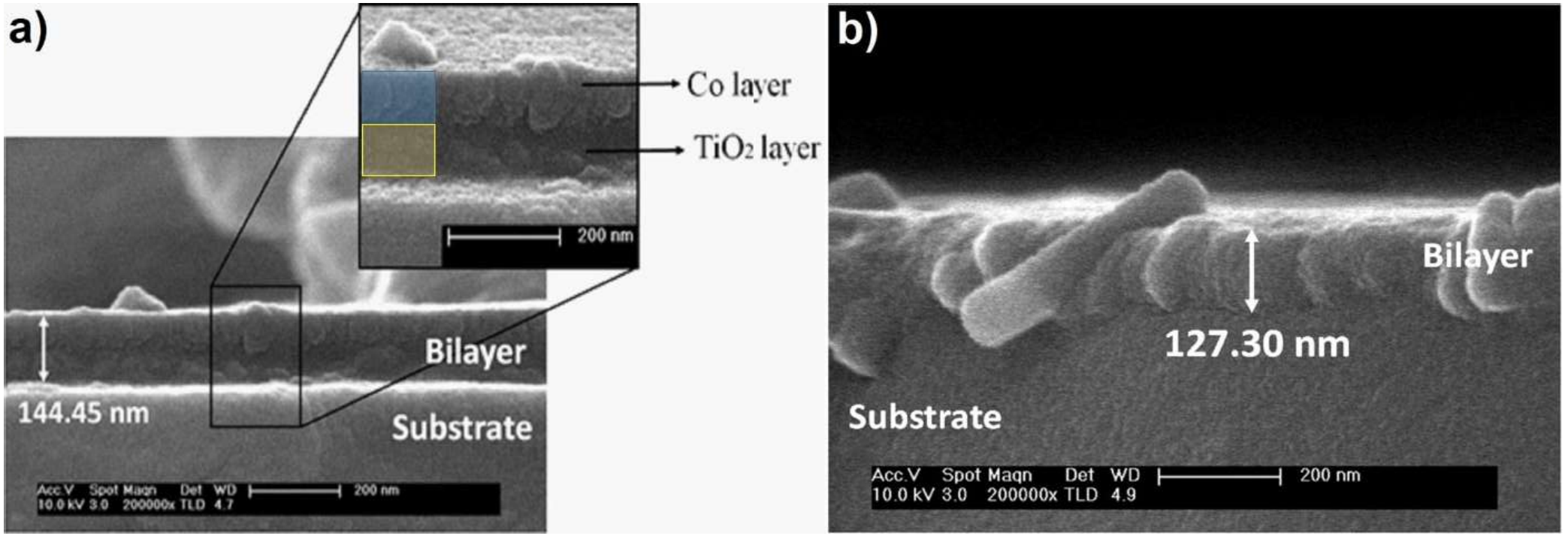
a)
Co layer
TiO2 layer
200 nm
Bilayer
144.45 nm
Substrate
Acc.V Spot Magn Det WD 200 nm
10.0 kV 3.0 200000x TLD 4.7
b)
Bilayer
127.30 nm
Substrate
Acc.V Spot Magn Det WD 200 nm
10.0 kV 3.0 200000x TLD 4.9

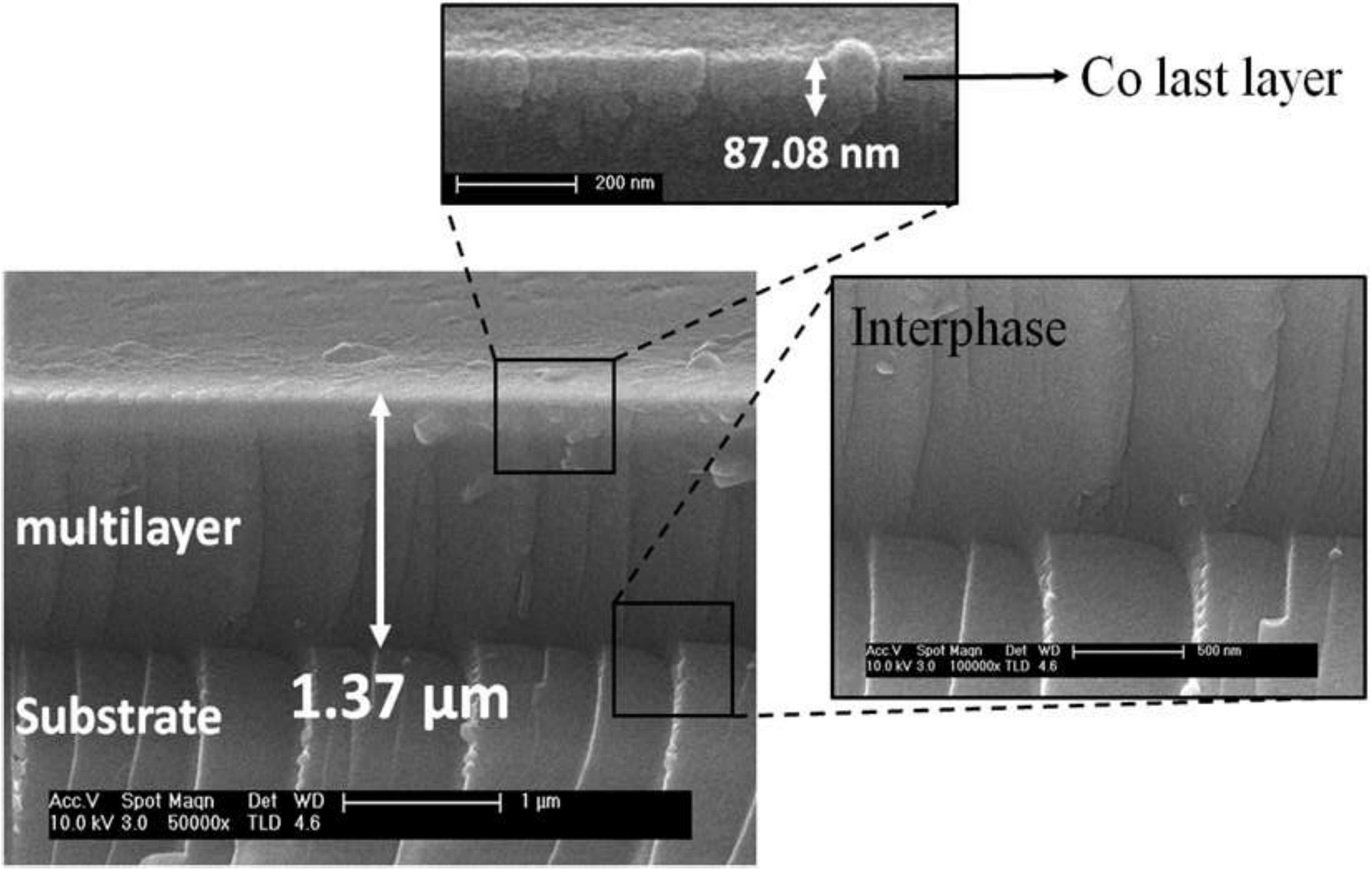
Co last layer
87.08 nm
200 nm
Interphase
Acc.V Spot Magn Det WD 500 nm
10.0 kV 3.0 100000x TLD 4.6
multilayer
1.37 µm
Substrate
Acc.V Spot Magn Det WD 1 µm
10.0 kV 3.0 50000x TLD 4.6

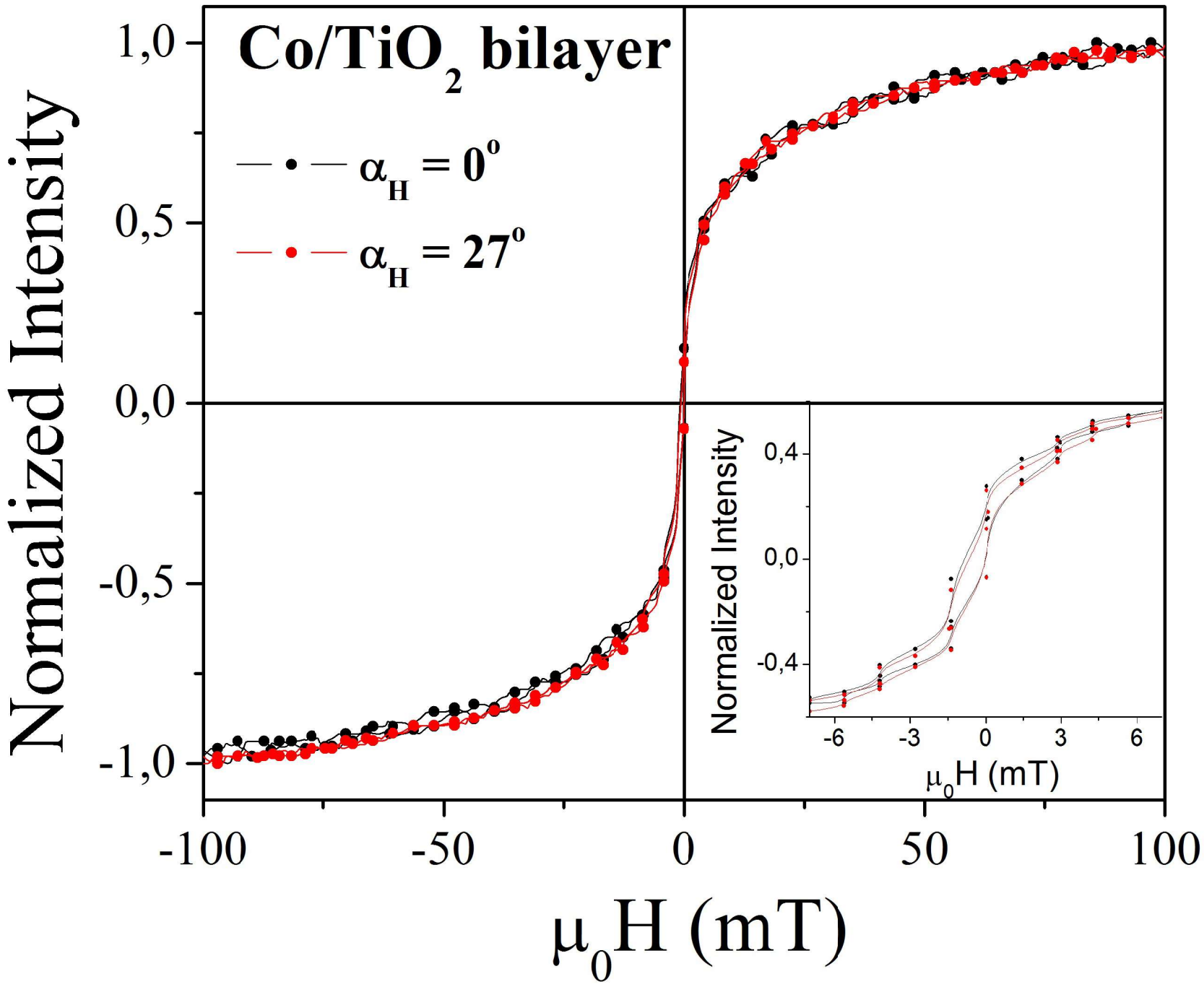
Co/TiO2 bilayer
αH = 0°
αH = 27°
Normalized Intensity
μ0H (mT)
1,0
0,5
0,0
-0,5
-1,0
-100
-50
0
50
100
0,4
0,0
-0,4
-6
-3
0
3
6

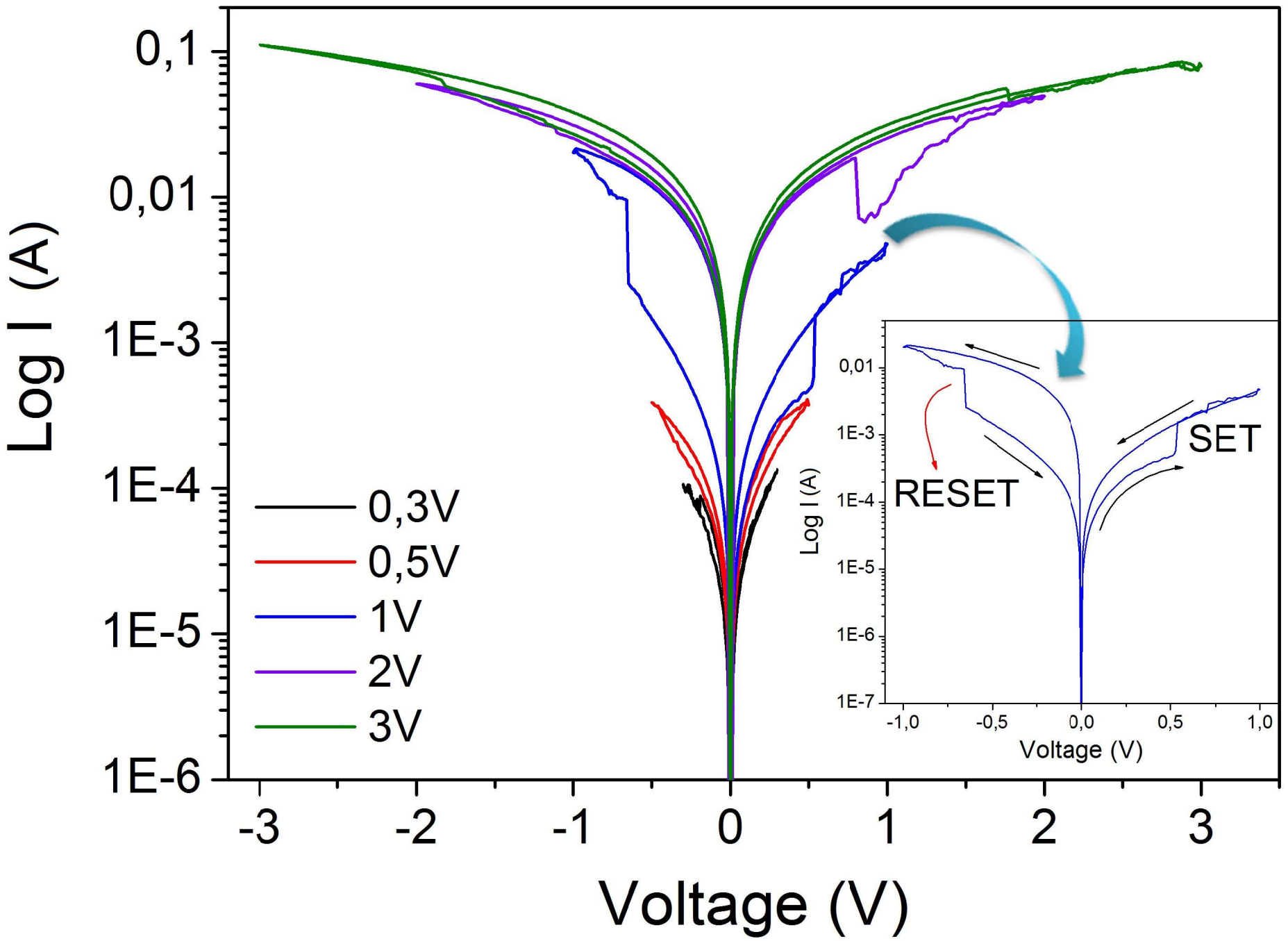
0,1
0,01
1E-3
1E-4
1E-5
1E-6
Log I (A)
-3
-2
-1
0
1
2
3
Voltage (V)
0,3V
0,5V
1V
2V
3V
0,01
1E-3
1E-4
1E-5
1E-6
1E-7
Log I (A)
RESET
SET
-1,0
-0,5
0,0
0,5
1,0
Voltage (V)

	Layer	Thickness - RBS ($10^{15}\ atoms/cm^2$)	Thickness - SEM (nm)
T_s = 293K	Co-O	25	-
	Co	80	75.50
	TiO_2	145	68.95
T_s = 473K	TiO_2-Co	150	127.30
	Ga-O	160	-